 doi:10.20944/preprints202102.0098.v1

Model membrane interactions and biological activity of a naphthalimide-containing BP100

Gustavo Penteado Battesini Carretero[1], Greice Kelle Viegas Saraiva[1], Magali Aparecida Rodrigues[1], Sumika Kiyota[3], Marcelo Porto Bemquerer[2], Hernan Chaimovich*[1], Iolanda Midea Cuccovia[1*].

1. Departamento de Bioquímica, Instituto de Química, Universidade de São Paulo, São Paulo, Brasil.

2. Embrapa Recursos Genéticos e Biotecnologia, Parque Estação Biológica, Brasília, Brasil

3. Laboratório de Bioquímica de Proteínas e Peptídeos, Instituto Biológico, São Paulo, Brasil

*Correspondence to Hernan Chaimovich, hchaimo@usp.br or

Iolanda Midea Cuccovia: imcuccov@iq.usp.br

Keywords: Antimicrobial peptide; BP100; Model membranes; Spectroscopy; Calorimetry; Biological activity

 doi:10.20944/preprints202102.0098.v1

Abstract

In a large variety of organisms, antimicrobial peptides (AMPs) are primary defences against pathogens. BP100 (KKLFKKILKYL-NH2), a short, synthetic, and cationic AMP, is active against bacteria and displays low toxicity towards eukaryotic cells. BP100 acquires an α-helical conformation upon interaction with membranes and increases membrane permeability. Despite the volume of information available, the mechanism of action of BP100, the selectivity of its biological effects, and its applications are far from consensual. In this work, we synthesized a fluorescent BP100 analog containing naphthalimide linked to its N-terminal end, Napht-BP100 (Napht-AAKKLFKKILKYL-NH2). The fluorescence properties of naphthalimides, especially their spectral sensitivity to microenvironment changes, are well established, and their biological activities against different types of cells are known. A wide variety of techniques were used to demonstrate that a-helical Napht-BP100 was bound and permeabilized POPC and POPG LUV. Napht-BP100, different from that observed for BP100, was bound to, and permeabilized POPC LUV. With zwitterionic (POPC) and negatively charged (POPG) containing LUVs, membrane surface high peptide/lipid ratios triggered complete disruption of the liposomes in a detergent-like manner. This disruption was driven by charge neutralization, lipid aggregation, and membrane destabilization. Napht-BP100 also interacted with double-stranded DNA, indicating that this peptide could also affect other cellular processes in addition to membrane destabilization. Napht-BP100 showed superior antibacterial activity, increased hemolytic activity compared to BP100, and may constitute an efficient antimicrobial agent for dermatological use. By conjugating BP100 and naphthalimide antimicrobial properties, Napht-BP100 was bound more efficiently to the bacterial membrane and could destabilize the membrane and enter the cell by interacting with its cytoplasm- exposed DNA.

Preprints (www.preprints.org) | NOT PEER-REVIEWED | Posted: 2 February 2021 doi:10.20944/preprints202102.0098.v1

1. Introduction

Antimicrobial peptides (AMPs) can destroy or inhibit the growth of bacteria, fungi, and viruses [1]. AMPs are ubiquitous components of the innate immune system and act as endogenous antibiotics [2, 3, 4, 5]. AMPs are positively charged and display a hydrophobicity index and hydrophobic moment, compatible with interactions with the bacterial membrane [6, 7]. The antibacterial activity of AMPs arises from electrostatic interactions with bacterial membranes, rich in negatively charged components such as phosphates, lipopolysaccharides from gram-negative bacteria, or lipoteichoic acids present in gram-positive bacteria. As the negative charge density of mammalian cell membranes is lower than that of bacteria, the electrostatic component is the main element of selectivity towards bacteria in cationic peptides' action [3, 4, 5, 6].

Peptide flip and hydrophobic residue exposure to the membrane interior [8] may follow electrostatic binding [8]. AMPs, in addition to the high density of positively charged side chains, contain tryptophan, tyrosine, and phenylalanine, with a high affinity to the membrane interface [2, 4, 5, 9]. After interaction with the membrane, the AMPs hydrophobic/hydrophilic topological distribution acquires a secondary structure that provides the peptide with a spatial amphipathic character, favoring the interaction with the membrane interface [4, 7]. Dehydration of the hydrophobic moieties, and not just the electrostatic components, can determine the bonding selectivity of AMPs to bacterial membranes [10].

Preprints (www.preprints.org) | NOT PEER-REVIEWED | Posted: 2 February 2021 doi:10.20944/preprints202102.0098.v1

Badosa and coworkers designed a series of AMP's to identify antimicrobial structure/potency relationships [11]. BP100 (KKLFKKILKYL-NH_2) (**Figure 1A**) combines the properties of melittin and cecropin A, acts by inhibiting the growth bacteria, exhibits low toxicity, high therapeutic index, and low sensitivity to degradation [12]. Atomic force microscopy showed that BP100 destroys the bacterial outer envelope at a minimum inhibitory concentration (MIC) of 3 μM [13]. The extent of damage is related to peptide binding and neutralization of the cell membrane's surface charge. Circular dichroism (CD) and *in silico* analysis showed that the membrane-bound form of BP100 had an α-helix content of 61% [13, 14, 15, 16, 17]. The acquisition of a helical secondary structure results in an amphipathic structure, ideal for a peptide/negatively charged lipid bilayer interaction. Circular-oriented dichroism (OCD) and solid-state nuclear magnetic resonance (SS-NMR) of BP100 labeled with ^{19}F showed that the highly mobile helix is positioned on the membrane with its long axis parallel to the membrane surface [16]. After an initial electrostatic driven approach, helical structured BP100 accommodates at the interface by flipping along its helix longer axis and inserting the hydrophobic side into the membrane hydrophobic acyl chains. Two other relevant phenomena regarding binding and flipping processes were also accessed: negative lipid clustering and peptide dehydration [8]. Microorganisms, or transformed cell disruption by BP100, and several BP100 analogs, and the effects resulting from groups linked to the parental peptide [17, 18], were analyzed [18].

Here, we present biophysical and biological studies of a naphthalimide-conjugated BP10 peptide (1,8-Naphthalimide-AAKKLFKKILKYL-NH_2, NAPHT-BP100) (**Figure 1**). Naphthalimide (1H-benzo [de] isoquinoline-1,3-(2H)-dione)

Preprints (www.preprints.org) | NOT PEER-REVIEWED | Posted: 2 February 2021 doi:10.20944/preprints202102.0098.v1

and related compounds bind to DNA and exert antitumor, anti-inflammatory, antidepressant, antiprotozoal and antiviral activities [19, 20, 21, 22, 23]. Advances in the synthesis of naphthalimide analogs have made it possible to explore derivatives such as mono-naphthalimides, di-naphthalimides, and naphthalimides conjugated with other compounds that exhibited different degrees of antibacterial activity depending on the attributed modifications [24, 25, 26].

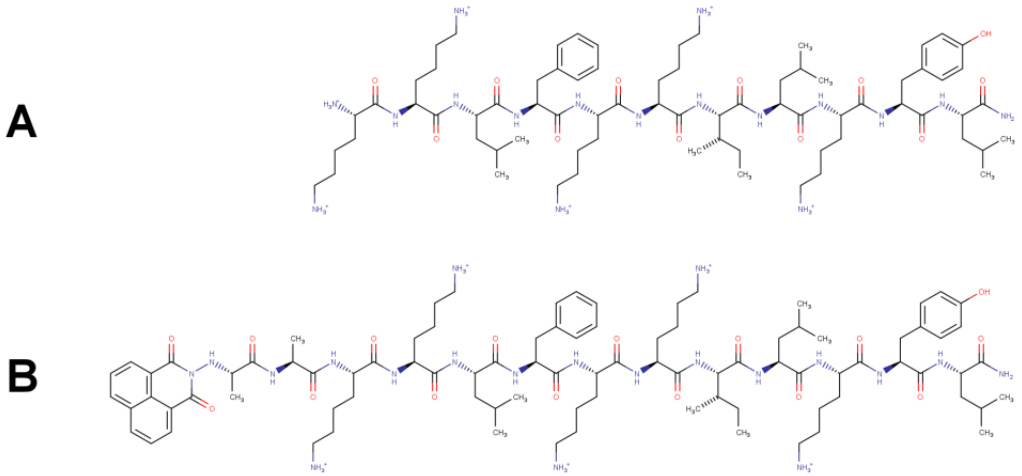

Figure 1. Structures of BP100 (KKLFKKILKYL-NH_2) **(A)** and Naphthalimide-AA-BP100 (1,8-Naphthalimide-AAKKLFKKILKYL-NH_2)(NAPHT-BP100) **(B)**.

However, the conjugating antimicrobial potential of an AMP and a DNA binding motif such as naphthalimide [27, 28, 29] has been overlooked. In this work, by taking advantaged biophysical and biological properties of naphthalimide, we aim to expand the understanding of NAPHT-BP100 and BP100 mechanism of action, and to obtain an improved antibacterial agent combining both membrane disruption and DNA binding capabilities.

 doi:10.20944/preprints202102.0098.v1

Our investigation focused on the NAPHT-BP100 secondary structure, membrane positioning, and bilayer lipid composition impact on binding, thermodynamics of NAPHT-BP100/membrane association, lipid organization, membrane surface charge, and peptide-induced liposome size changes. Binding data were correlated with NAPHT-BP100-induced vesicle permeabilization, allowing NAPHT-BP100 activity rationalization. The peptide-DNA interaction was also investigated. Biological activity was examined by determining the minimum inhibitory peptide concentration against gram-negative and gram-positive bacterial species. Hemolytic activity against human red blood cells was measured as a mean of evaluating peptide toxicity.

Preprints (www.preprints.org) | NOT PEER-REVIEWED | Posted: 2 February 2021 doi:10.20944/preprints202102.0098.v1

2. Material and Methods

2.1 Reagents

5(6)-Carboxyfluorescein (CF) (Sigma-Aldrich (St. Louis, MO), was purified, and the sodium salt was prepared and quantified as described previously [15]. 1-Palmitoyl-2-oleoyl-*sn*-glycero-3-phosphocholine (POPC), 1,2-dipalmitoyl-*sn*-glycero-3-phosphocholine (DPPC), 1-palmitoyl-2-oleoyl-sn-glycero-3-[phospho-rac-(1-glycerol)], sodium salt (POPG), and 1,2-dipalmitoyl-sn-glycero-3-[phospho-rac-(1glycerol)], sodium salt (DPPG) (Avanti Polar Lipids (Alabaster, AL)) were used as received. Double-stranded DNA pET-28a(+) vector (ds-DNA) was obtained from Sigma-Aldrich (St. Louis, MO).

2.2 Peptide synthesis

Peptides were synthesized by solid phase [30], using “Rink Amide” resin (Peptides International, Louisville, KY) for amidated peptides. Fmoc deprotection reactions were carried out with a 20% solution of 4-methylpiperidine in N,N-dimethylformamide (DMF) for 20 to 30 min (in two steps of 10 to 15 min). Coupling reactions were conducted with 1,3-diisopropylcarbodiimide (DIC) and ethyl-2-cyano-2-(hydroxyimino) acetate (Oxyma®) or [benzotriazol tetrafluoroborate-1-yloxy(dimethylamino)methylidene]-dimethylazanium (TBTU) and N,N´-diisopropylethylamine (DIEA) in DMF for 60 to 90 min. Deprotection and coupling steps were monitored by the ninhydrin reaction [30, 31]. After each deprotection and coupling step, the resin was washed three times with methanol (or 2-propanol) and DMF, consecutively.

Preprints (www.preprints.org) | NOT PEER-REVIEWED | Posted: 2 February 2021 doi:10.20944/preprints202102.0098.v1

Modifications with naphthalic anhydride were carried out as the final stage of solid-phase synthesis [32, 33]. modifications of the peptides with 1,8-naphthalic anhydride were carried out in DMF at 60 °C for 24 h under orbital agitation, with a molar excess of four to eight times the anhydride in relation to the amino terminal group. A re-coupling was carried out with the addition of DIC in equimolar amounts in relation to naphthalic anhydride at 60 °C for 24 h. After the synthesis was completed, the final deprotection and cleavage reactions were carried out in a solution of trifluoroacetic acid in the presence of nucleophiles (e.g., triisopropylsilane, 1,2-ethanedithiol, thioanisole) as carbocation scavengers, for 120 minutes, at room temperature. After precipitation of the crude material with diisopropyl ether and four to six washes with the same solvent, the peptide was collected by filtration in a porous plate funnel, extracted with water or aqueous acetonitrile solution and lyophilized.

Peptides were purified by reversed-phase chromatography on a semi-preparative column with an octadecylsilane matrix (C18, 250 × 22 mm, 10 µm, 300 Å) from Grace-Vydac (Columbia, MD) at a flow rate of 9.0 mL/min at room temperature. The purity analysis of the synthetic peptides was conducted by reversed-phase chromatography using an analytical column octadecylsilane (C18, 250 × 4.6 mm, 5 µm) Grace-Vydac, using a flow rate of 1.0 mL/min at room temperature (**Figures SM-1 and SM-2**). The elution, both for the analytical method and for the preparation, was carried out with gradients of increasing concentration of acetonitrile in water, in the presence of trifluoroacetic acid as an ionic pair forming cationic groups [34] with detection at 220 nm. The identity of the products was verified by mass spectrometry in the MALDI-TOF mode (Autoflex Speed, Bilerica, MA) (**Figures SM-3 and SM-4**).

Preprints (www.preprints.org) | NOT PEER-REVIEWED | Posted: 2 February 2021 doi:10.20944/preprints202102.0098.v1

2.3 Peptide and ds-DNA solutions

Peptide solutions were prepared by weighing the dry powder and solubilizing it in autoclaved deionized water. Peptide concentrations were measured using an N-1000 Nanodrop spectrophotometer (Thermo Fisher Scientific Wilmington, DE), considering the tyrosine residue absorbance at 275 nm ($\varepsilon_{275\ nm}$ = 1400 $M^{-1}.cm^{-1}$) for BP100 and naphthalimide moiety absorbance at 342 nm for NAPHT-BP100 ($\varepsilon_{342\ nm}$ = 12900 $M^{-1}.cm^{-}1$). The NAPHT-BP100 UV absorption spectrum was recorded in a Varian Cary 50 UV/Vis Spectrophotometer (Agilent Technologies, Santa Clara, CA) from 220 nm to 500 nm.

The DNA concentration (in base pair) was determined spectrophotometrically using an N-1000 Nanodrop spectrophotometer at 260 nm (ε_{260} = 0.020 $(\mu g/mL)^{-1}.cm-1$), and the ratio between the absorbance at 260 and 280 nm was registered to attest the sample purity.

2.4 Model membrane preparation

Lipid stock solutions were prepared in chloroform and quantified by measuring the phosphate concentration [35]. Lipid films with the desired amount and molar ratios were prepared by mixing an adequate volume of each lipid stock solution, followed by solvent evaporation under a stream of argon, and complete drying under vacuum for at least two h.

Lipid films were suspended in aqueous Tris-HCl 10 mM, pH 7.4, buffer solution yielding multilamellar vesicles (MLV). Large unilamellar vesicles (LUV) with a hydrodynamic diameter of 100 nm were obtained by extrusion of MLV trough polycarbonate membranes (Millipore, MA, USA) in a LiposoFast syringe-driven extruder (AVESTIN, Ottawa, Canada).

Preprints (www.preprints.org) | NOT PEER-REVIEWED | Posted: 2 February 2021 doi:10.20944/preprints202102.0098.v1

For the CF leakage assay, LUV was prepared in Tris-HCl 10 mM, pH 7.4 buffer containing CF 50 mM. Solution-free CF was separated from the LUV by size-exclusion chromatography using a pre-packed Sephadex G-25 filter column (GE Healthcare, Buckinghamshire, UK) equilibrated with 10 mM Tris-HCl buffer, pH 7.4, with NaCl 300 mM. The Collected lipid suspension was quantified by measuring phosphate [35].

2.5 Fluorescence

Steady-state fluorescence spectra of NAPHT-BP100 in Tris-HCl 10 mM, pH 7.4 buffer, containing or not NaCl 300 mM, were obtained using a Hitachi F7000 spectrofluorometer (Hitachi, Tokyo, Japan) at 25, 45 and 65 °C. Naphthalimide moiety fluorescence emission was recorded from 345 to 550 nm, at a rate of 240 nm/min, and exciting the sample at 342 nm. The Initial peptide concentration was 5, 10, 20, or 40 µM, and lipid concentration was varied from 0 to 2.8 mM.

Peptide-DNA interaction was studied by varying DNA concentration from 0 to 15 ng/µL. Spectra of Tris-HCl 10 mM, pH 7.4, buffer, either containing or without NaCl 300 mM, and of the vesicles in buffer without peptide, taken under the same conditions, were subtracted from the peptide spectra for correction. In addition, spectra were also corrected by peptide dilution as the lipid addition proceeded.

2.6 Circular dichroism

Circular dichroism spectra of NAPHT-BP100 in Tris-HCl 10 mM, pH 7.4 buffer were obtained using a Jasco J-720 spectropolarimeter (Jasco, Easton, MD) at room temperature. Samples were placed in a 0.1 cm optical length quartz cells

Preprints (www.preprints.org) | NOT PEER-REVIEWED | Posted: 2 February 2021 doi:10.20944/preprints202102.0098.v1

and spectra were scanned from 190 to 260 nm, at a rate of 50 nm/min, with bandwidth of 2 nm, step resolution of 0.5 nm, response time of 2 seconds, and the final spectrum was the average of six scans. The Initial peptide concentration was 20 µM, and lipid concentration was varied from 0 to 1.6 mM. The Spectra of the buffer and the vesicles in buffer were obtained under the same conditions and subtracted from the CD spectra of the peptide. Finally, the ellipticity intensities (θ, mdeg) were normalized to molar ellipticity ([θ], deg.cm^2.dmol^{-1}) using **Equation** 1 to eliminate the spectral dependence on optical length, peptide concentration and number of residues.

$$[\theta] = \theta / (10*C*l*N) \qquad \textbf{Equation 1}$$

where C is peptide concentration in mol/L, N is the number of residues, and l is the cell optical length in cm.

2.7 Dynamic light scattering (DLS)

LUV hydrodynamic diameter and size distribution, and electrophoretic mobility were measured in a Zetasizer Nano apparatus equipped with a 633 nm laser (Malvern, Worcestershire, UK). The LUV surface zeta potential was calculated from the electrophoretic mobility using Henry's equations (**Equations 2 and 3**).

$$UE = 2\,Ɛ\,Zf(ka)/3η \qquad \textbf{Equation 2}$$

$$ζ = η\,UE / Ɛ \qquad \textbf{Equation 3}$$

where ζ is the zeta potential, UE is the electrophoretic mobility, Ɛ the dielectric constant of water, f(ka) is Henry's function, and η is the viscosity of the medium.

Preprints (www.preprints.org) | NOT PEER-REVIEWED | Posted: 2 February 2021 doi:10.20944/preprints202102.0098.v1

LUV composed of POPC:POPG (50:50, mol:mol) was prepared in Tris-HF 10 mM, pH 7.4, buffer. The Lipid concentration remained fixed at 50 µM throughout the experiment and peptide concentration was varied from 0 to 32 µM.

2.8 Isothermal titration calorimetry (ITC)

ITC measurements were performed at 25 °C in a MicroCal VP-ITC isothermal titration calorimeter (MicroCal, Northampton, MA) by loading a 3 to 6 mM LUV suspension in the syringe and titrating a 40 µM peptide solution in Tris-HCl 10 mM, pH 7.4 buffer, placed in the cell (V_{Cell} = 1.54 mL). Titration consisted of 25 sequential injections of 10 µL of the lipid suspension into the cell every five min. Samples were previously degassed and a reference cell filled with demineralized water.

2.9 Differential scanning calorimetry

The phase transition temperature (Tm), cooperativity ($\Delta T_{1/2}$) and enthalpy (ΔH) of DPPC:DPPG (70:30, molar ratio) MLV were determined on a MicroCal VP-DSC differential scanning microcalorimeter (MicroCal, Northampton, MA). Samples were prepared by suspending the lipid film in previously degassed Tris-HCl 10 mM, pH 7.4 buffer solution with 0; 6; 12 and 25 µM of the peptide, to a final lipid concentration of 1.0 mM. Measurements were performed under a constant external pressure of 35 psi in order to avoid bubble formation. samples were heated at a constant scan rate of 12 °C/h and the temperature was scanned from 15 to 60 °C. Tris-HCl 10 mM, pH 7.4, buffer solution was used as a reference. The data were analyzed the Origin 8.5 program.

2.10 Model membrane vesicle permeabilization

Preprints (www.preprints.org) | NOT PEER-REVIEWED | Posted: 2 February 2021 doi:10.20944/preprints202102.0098.v1

CF leakage assays were performed in a black-bottom opaque 96-well plate in which a two-fold serial dilution of the peptide in Tris-HCl 10 mM, pH 7.4, buffer with NaCl 300 mM was mixed with the same volume of CF containing LUV suspension with a lipid concentration of 40 µM. The Final peptide concentration ranged from 16 to 0.125 µM and the final lipid concentration was 20 µM. CF fluorescence emission increase due to vesicle permeabilization by the peptide was measured at 520 nm, exciting the sample at 490 nm for 60 minutes, at 37 °C, in a Bio-Tek Synergy HT Microplate Reader (Bio-Tek, Winooski, VT). To access the fluorescence emission regarding total permeabilization of the LUV, 1.5 µL of a solution of polidocanol 10% (v/v) was added to each well and used as positive control to achieve 100% permeabilization; buffer solution was used as negative control and to ensure that no spontaneous leakage occurred in a significant extent. The percentage of CF leakage in each well was calculated using **Equation 4**.

$$\text{CF Leakage (\%)} = 100 \times (F_P - F_0) / (F_T - F_0) \qquad \textbf{Equation 4}$$

where F_P is the fluorescence emission intensity of the well containing the peptide after 30 min, and F_0 and F_T are the fluorescence emission intensities of the negative (before peptide addition) and positive (after polidocanol addition and 100 % permeabilization) control, respectively.

2.11 Minimum inhibitory concentration assay

The assays for determining the minimum peptide concentration necessary to inhibit bacterial growth were carried out according to Wiegand et al. [36]. *Escherichia coli* (ATCC 25922), *Staphylococcus aureus* (ATCC 25923)

Preprints (www.preprints.org) | NOT PEER-REVIEWED | Posted: 2 February 2021 doi:10.20944/preprints202102.0098.v1

and *Bacillus subtilis* (PY79) bacterial species were tested for the assays, which were carried out in triplicate.

Initially, 10 mL of MHB medium was inoculated with a small number of bacteria from a single colony deposited on a solid agar plate. The bacteria were then incubated overnight at 37 °C and 250 rpm shaking. The cell suspension was then diluted 50 times in MHB medium and incubated again at 37 °C. Upon reaching an optical density at 600 nm of approximately 0.4, the cell suspension was again diluted 250 times in MHB medium, resulting in a bacterial suspension of 10^6 CFU/mL. In parallel, in a 96-well polypropylene U bottom plate, a two-fold serial dilution of the peptide in MHB medium was prepared with two times the desired final peptide concentration, ranging between 32 and 0.05 µM and a volume of 50 µL. Next, 50 µL of the cell suspension was added to the peptide solution, resulting in a 5.10^5 CFU/mL bacterial suspension, and the plate was incubated for 18 h at 37 °C. MHB inoculated with 50 µL of the bacterial suspension was used as a positive control and sterile MHB as a negative control. After 18 h, bacterial growth was visually checked to access the MIC.

2.12 Hemolytic activity

The hemolytic activity of BP100 and NAPHT-BP100 was evaluated following Mojsoska *et al*. [37]. Five milliliters of human blood obtained from healthy volunteers were mixed with 40 mL of sterile phosphate buffered saline solution (140 mM NaCl, 10 mM phosphate, pH 7.4, PBS) and centrifuged for 10 minutes at 1500 rpm, equivalent to 500 *g*. The supernatant was removed and the cells were washed (x3).

Preprints (www.preprints.org) | NOT PEER-REVIEWED | Posted: 2 February 2021 doi:10.20944/preprints202102.0098.v1

Next, 9.7 ml of PBS was added, resulting in a 3% cell volume suspension. A 96-well polypropylene plate (Corning, NY, USA) was previously prepared with serial dilutions of the peptide in PBS at concentrations between 128 and 2 μM and a final volume of 50 μL. For the assay, 50 μL of the 3% red blood cell suspension was added to each well of the plate containing the peptide dilutions, yielding a final suspension of 1.5% RBC. As a negative control, sterile PBS was used, and as a positive control, to achieve 100% hemolysis, 0.1% (v/v) Triton X-100 was added. The plate was incubated under shaking for 3 h at 37 °C and then centrifuged at 1200 rpm (400 g) for 10 min. The supernatant containing the hemoglobin released by the action of the peptides was transferred to a flat-bottomed 96-well polystyrene plate (Greiner Bio-One, Kremsmünster, Austria). The absorbance at 414 nm was then measured on a Synergy HT plate reader (Bio-Tek, Winooski, VT, USA). The percentage of hemolysis was calculated based on the absorbance measured using **Equation 5**:

$$\text{Hemolysis (\%)} = 100 \times (A_{PEP} - A_{NEG}) / (A_{POS} - A_{NEG}) \qquad \textbf{Equation 5}$$

where A_{PEP}, A_{NEG} and A_{POS} refer to the sample's absorbance with the peptide, and the positive and negative controls, respectively.

Preprints (www.preprints.org) | NOT PEER-REVIEWED | Posted: 2 February 2021 doi:10.20944/preprints202102.0098.v1

3. Results

3.1 UV-absorption and fluorescence – NAPHT-BP100 membrane and ds-DNA binding

The NAPHT-BP100 UV absorption spectrum shows three characteristic peaks at 343, 275 and 230 nm corresponding to the absorption from the naphthalimide moiety, the tyrosine side chain, and the peptide bond, respectively (**Figure 2 A**). From this result, the maximum absorption wavelength of the naphthalimide moiety was determined and used as the excitation wavelength to study peptide fluorescence properties.

The emission spectrum of NAPHT-BP100 presented peaks at 385 and 400 nm, and the fluorescence emission intensity was lower at high salt concentrations (**Figure 2 B**). The fluorophore was likely less hydrated in 0.3 M NaCl, causing a decrease in fluorescence emission intensity but no peak displacement [38]. As the temperature increased from 25 to 65 °C, the fluorescence emission of NAPHT-BP100 in solution decreased slightly with no changes in peak positioning or spectral shape (Figure **SM-5 A**).

Upon POPC: POPG (50:50, molar ratio) LUV addition, NAPHT-BP100 fluorescence emission intensity decreased, and both emission peaks were blue-shifted by 10 nm (**Figure 2 B, C**). Blue shifts and decrease in emission intensity decrease are associated with fluorophore transfer to a more hydrophobic environment [38]. The emission spectra of membrane-bound NAPHT-BP100 in high or low salt were similar (**Figure 2 B**), suggesting that the fluorophore was inside the membrane.

Preprints (www.preprints.org) | NOT PEER-REVIEWED | Posted: 2 February 2021 doi:10.20944/preprints202102.0098.v1

The free/bound ratios of membrane association of NAPHT-BP100 were calculated from the lipid concentration-dependence of the fluorescence emission, assuming a two-state model. (**Figure 2 C, D, and E**).

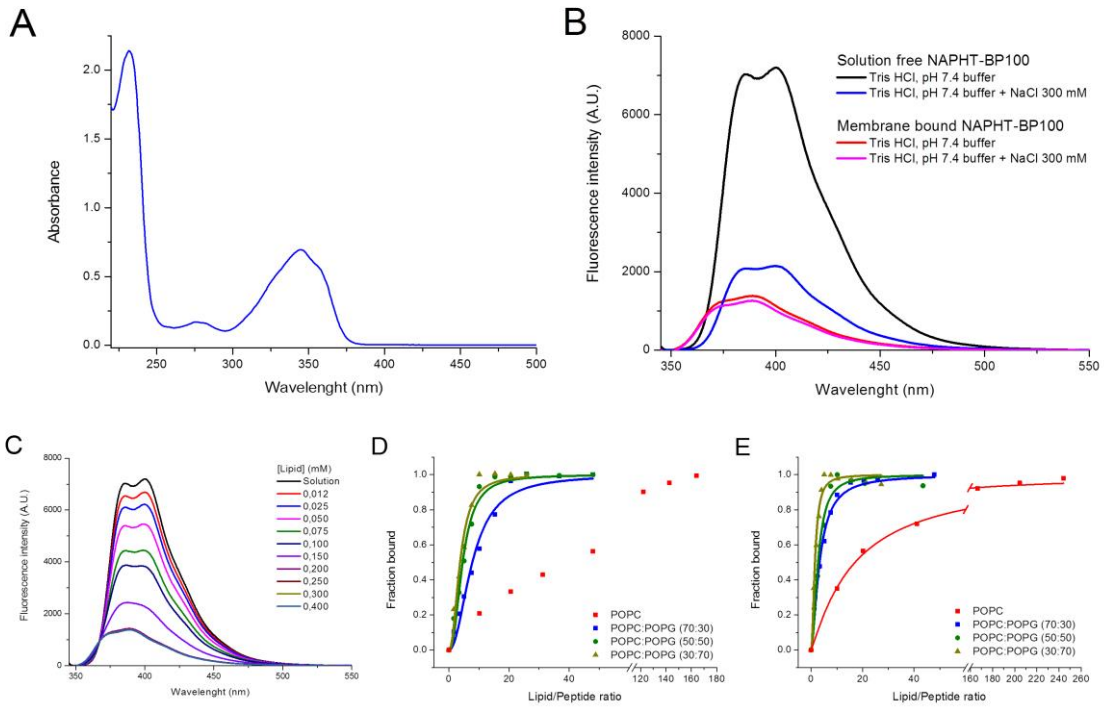

Figure 2. Analysis of NAPHT-BP100 UV absorption, fluorescence and lipid binding. **(A)** NAPHT-BP100 UV absorption spectrum. Peptide concentration 55 µM. **(B)** Fluorescence spectra of NAPHT-BP100 in solution and bound to POPC:POPG (50:50, molar ratio) LUV in Tris-HCl 10 mM, pH 7.4, buffer with or without NaCl 300 mM. **(C)** Fluorescence spectra of NAPHT-BP100 in solution and with POPC:POPG (50:50) LUV in Tris-HCl 10 mM, pH 7.4, buffer. **(D)** Binding curve of NAPHT-BP100 to LUV in Tris-HCl 10 mM, pH 7.4, buffer. **(E)** Binding curve of NAPHT-BP100 to LUV in Tris-HCl 10 mM, pH 7.4, buffer with NaCl 300 mM. The peptide concentration was 20 µM and temperature 25 °C. $\lambda_{Exc} = 342$ nm.

The addition of POPC-LUV to NAPHT-BP100 in low or high salt, reaching lipid/peptide ratios up to 240, also triggered a decrease, demonstrating peptide-membrane interactions (**Figure SM-6**). However, only at high salt full binding was observed (Figure 2D).

Preprints (www.preprints.org) | NOT PEER-REVIEWED | Posted: 2 February 2021 doi:10.20944/preprints202102.0098.v1

Interaction between NAPHT-BP100 and LUV containing 30 to 70 mol% of POPG occurs primarily due to electrostatic interactions between the negatively charged bilayer and the positively charged peptide [15, 17]. The addition of LUV to NAPHT-BP100 decreased fluorescence emission to a minimum where further lipid additions ceased to produce spectral change, indicating that the peptide was fully liposome-bound.

We calculated the lipid/peptide ratio from the binding isotherms, where 50 % of NAPHT-BP100 was LUV-bound (L/P_{50}). (**Figure 2 D and E**). The addition of POPG to the LUV lipids increased, as expected [15], NAPHT-BP100 binding, and the binding extent increased with salt (**Table 1**). L/P_{50} was less dependent on the POPG contents at high salt. Note the differences between peptide affinity to LUV with 30 and 50 mol% of POPG (Table 1). Increasing the temperature from 25 to 65 °C did not change the binding degree (**Figure SM-5 B**).

Table 1. L/P_{50} ratios were obtained by fluorescence, CD, and ITC* for LUVs with different ratios of POPC:POPG

	Peptide	**NAPHT-BP100**		**NAPHT-BP100**	**NAPHT-BP100**	**BP100****	**BP100****
	Method	**Fluorescence**		**CD**	**ITC**	**CD**	**Fluorescence**
LUV POPG content (%)		**No salt**	**NaCl 0.3 mM**	**No salt**	**No salt**	**No salt**	**No salt**
0		No fit	17	No fit	- - -	No binding	No binding
30		6.4 ± 1.0	3.3	7.3	11.1	13.2	15.2
50		4.0 ± 0.4	2.5	3.9	5.2	5.1	5.8
70		3.2 ± 0.7	1.6	3.7	- - -	- - -	- - -

*All measurements performed at 25 °C.
**From Carretero et al. [17].

Preprints (www.preprints.org) | NOT PEER-REVIEWED | Posted: 2 February 2021 doi:10.20944/preprints202102.0098.v1

Naphthalimide derivative fluorescence spectra are also sensitive to the interaction of these molecules with mono-and oligonucleotides [39]. Taking advantage of this property, NAPHT-BP100 binding to ds-DNA was investigated by fluorescence spectroscopy (**Figure 3**). The presence of ds-DNA in solution triggered a decrease in naphthalimide fluorescence emission attesting peptide-DNA interaction (**Figure 3 A**), and the degree could be further explored by varying the ds-DNA concentration to obtain a binding isotherm in the same way as accomplished in the studies with LUV (**Figure 3 B**).

NAPHT-BP100 bound to a large extent to ds-DNA, considering that complete binding was achieved at a ds-DNA base pair/NAPHT-BP100 ratio of 2.5. At this ratio, NAPHT-BP100 five positively charged groups were stoichiometrically neutralized by five negatively charged phosphate groups of the 2.5 ds-DNA base pairs. In this case, both charge neutralization and naphthalimide intercalation in the DNA [27] would contribute to a large degree of interaction.

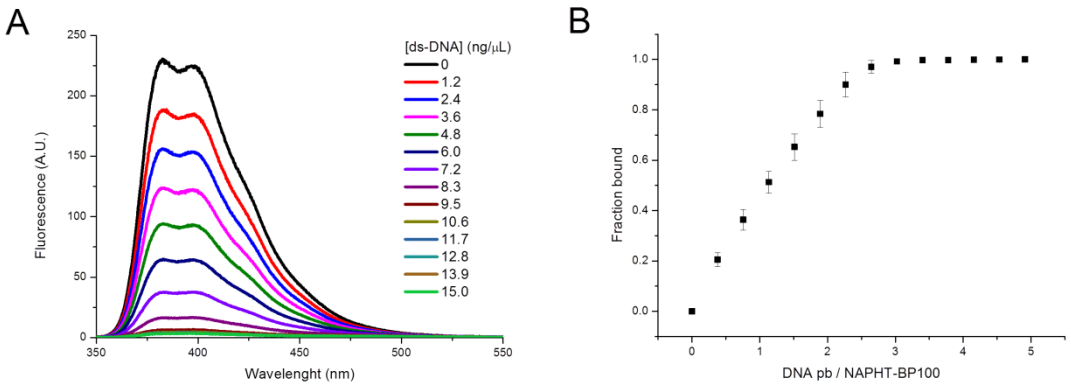

Figure 3. Analysis of NAPHT-BP100/ds-DNA binding. **(A)** Fluorescence spectra of NAPHT-BP100 in solution and at different concentrations of ds-DNA in Tris-HCl 10 mM, pH 7.4, buffer. **(B)** Binding curve of NAPHT-BP100 to ds-DNA in Tris-HCl 10 mM, pH 7.4, buffer. The peptide concentration was 5 μM and temperature 25 °C.

Preprints (www.preprints.org) | NOT PEER-REVIEWED | Posted: 2 February 2021 doi:10.20944/preprints202102.0098.v1

3.2 Circular Dichroism

NAPHT-BP100 in aqueous solution displayed a far-UV CD spectrum with a negative peak at 198 nm and a negative and low-intensity peak centered around 230 nm, indicating that the peptide was in a random/flexible structure with a low degree of helical secondary structure (**Figure 4 A**). This conformation was different from that of BP100 that, under the same conditions, displays a completely flexible structure [15, 17]. Naphthalimide addition to the N-terminus of BP100 in NAPHT-BP100 induced the attainment of some degree of secondary structure.

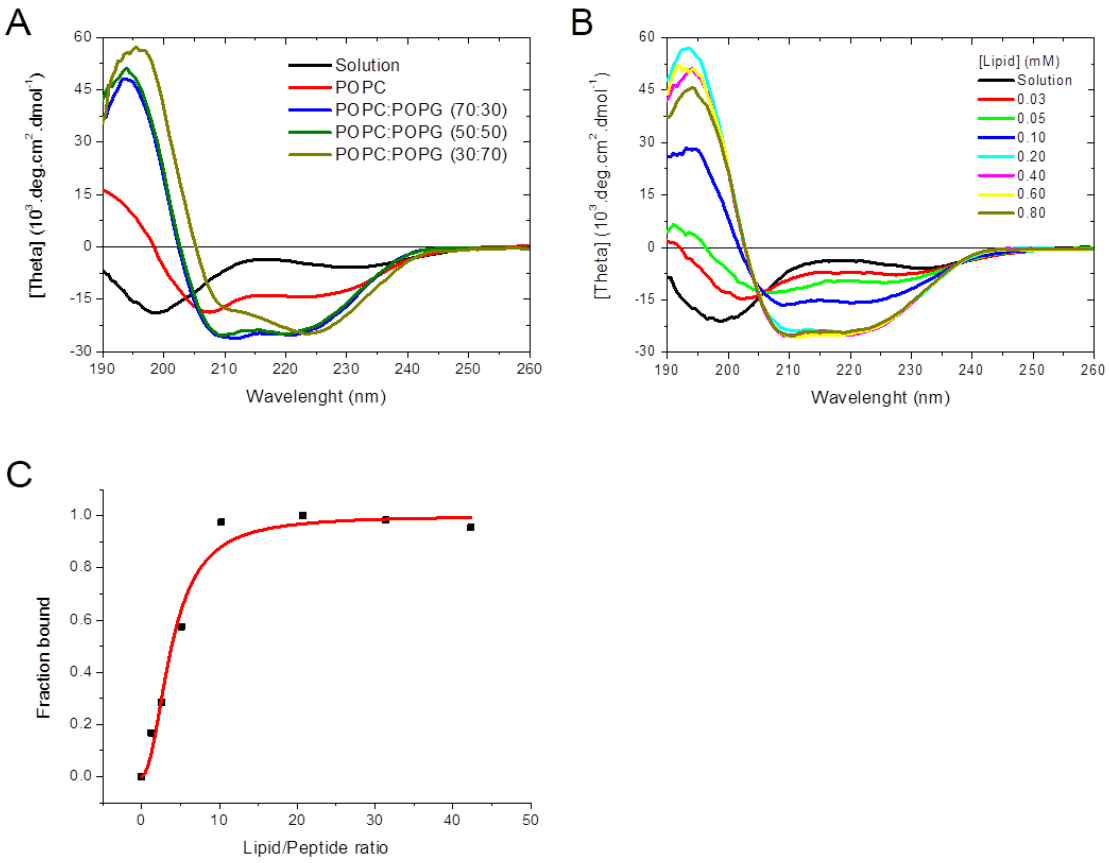

Figure 4. (A) CD spectra of NAPHT-BP100 in solution and in the presence of 0.6 mM of LUVs composed of POPC and POPG at different proportions, in Tris-HCl 10 mM, pH 7.4 buffer. **(B)** CD spectra of NAPHT-BP100 in solution with different concentrations of POPC:POPG (50:50, molar ratio) in Tris-HCl 10 mM, pH 7.4 buffer. **(C)** Binding curve of NAPHT-BP100 to POPC:POPG (50:50,

Preprints (www.preprints.org) | NOT PEER-REVIEWED | Posted: 2 February 2021 doi:10.20944/preprints202102.0098.v1

molar ratio) LUV in Tris-HCl 10 mM, pH 7.4 buffer. The peptide concentration was 20 µM and temperature 25 °C.

The CD spectra of NAPHT-BP100, with LUV (30, 50, or 70 mol% POPG), are typical of an α-helical secondary structure, displaying a positive peak at 195 nm and two negative bands at 208 and 222 nm (**Figure 4 A**). The interaction of NAPHT-BP100 and other related peptides [14, 15, 17]with negatively charged vesicles triggered a coil-to-helix transition. The 208/222 nm intensity peak ratio of the spectra of NAPHT-BP100 with 70 mol% of POPG LUV differed from the ratios calculated from the spectra of the peptide bound to LUV containing 30 or 50 mol% of POPG. These differences suggested that NAPHT-BP100, as discussed previously for BP100 [15], aggregated on the membrane surface and induced lipid clustering.

With LUV's composed of POPC, the NAPHT-BP100 CD spectrum changes indicated a coil-to-helix transition (**Figure 4 A**), but complete binding was not obtained even at a lipid/peptide ratio of 190. Previous SS-NMR results with BP100 showed that the membrane-bound form of BP100 and other analogs adopt a helical secondary structure regardless of the surface net charge [40].

The isodichroic point at 204 nm indicated that the NAPHT-BP100: POPG:POPC (1:1) LUV interaction was compatible with a two-state model for binding (**Figure 4 B**).

Peptide-membrane interactions between the different lipid systems studied and the techniques employed were analyzed from binding isotherms (**Figure 4 C, Table 1**). CD data indicated that peptide-membrane affinity increased with POPG content (**Table 1**).

Preprints (www.preprints.org) | NOT PEER-REVIEWED | Posted: 2 February 2021 doi:10.20944/preprints202102.0098.v1

CD spectral deconvolution allowed quantitative analysis of the secondary structure of NAPHT-BP100 (**Table 2**) [41]. In solution, NAPHT-BP100 displayed 81% of the flexible random coil structure (10.5 residues) and 19 % of α-helical secondary structure (2.5 residues). Binding to lipid membranes containing POPG-triggered a structural transition in which NAPHT-BP100 acquires approximately 75-83% of helical conformation (10 residues) and 17-25 % of its length remaining in a random coil structure. Interestingly, the bound form of NAPHT-BP100 in the presence of LUV containing 70% of POPG indicates the presence of 75% α-helix and 17% β-sheet secondary structures, supporting the notion that the peptide aggregated on the membrane surface, indicating that aggregation could occur through the formation of β-sheet structured segments. The NAPHT-BP100 spectrum in the presence of POPC LUV was not analyzed since complete peptide binding was not achieved, and thus no representative spectrum of the peptide bound form was obtained.

Table 2. Secondary structure contents of NAPHT-BP100 in solution and bound to LUV calculated from CD spectra.

Lipid	α-helix (%)	β-sheet (%)	Flexible (%)
None	19	0	81
POPC:POPG 70:30	76	6	18
POPC:POPG 50:50	83	0	17
POPC:POPG 30:70	75	17	8

3.3 Isothermal titration calorimetry

NAPHT-BP100 binding to LUV was exothermic (**Figure 5**). The Measured heat changes allowed for an analysis of the binding thermodynamics (**Table 3**).

Preprints (www.preprints.org) | NOT PEER-REVIEWED | Posted: 2 February 2021 doi:10.20944/preprints202102.0098.v1

The calorimetric data indicated that NAPHT-BP100 binding was driven by a negative enthalpy component and a positive entropy contribution (**Table 3**). Enthalpy variation can be ascribed to electrostatic interactions between NAPHT-BP100 and the membrane surface, while entropy variations are most likely related to peptide dehydration and hydrophobic interactions between peptide hydrophobic helix face and lipid acyl chains. Binding of some hydrotropic ions to zwitterionic interfaces is controlled by the dehydration of their hydrophobic moieties [42].

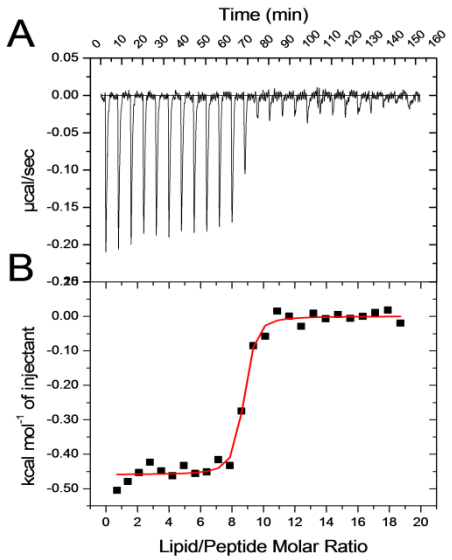

Figure 5. NAPHT-BP100 lipid binding by calorimetry. **(A)** Heat variation per second during titration of an NAPHT-BP100 peptide solution with a POPC:POPG (50:50) LUV suspension. **(B)** Integrated heat per mole of lipid at each injection as a function of lipid/peptide molar ratio. Measurements were performed at 25 °C, loading a 3 to 6 mM LUV suspension in the syringe and titrating a 40 µM peptide solution in Tris-HCl 10 mM, pH 7.4 buffer.

Preprints (www.preprints.org) | NOT PEER-REVIEWED | Posted: 2 February 2021 doi:10.20944/preprints202102.0098.v1

Table 3. Thermodynamic parameters of NAPHT-BP100-lipid interaction.

PG%	N (Lip/NAPHT-BP100)	ΔH (kcal/mol)	ΔS (cal/mol/K)	- T ΔS (kcal/mol)	ΔG (kcal/mol)	K (M^{-1})
30	21.7	- 5.4 ± 0.3	9.8 ± 2.5	- 2.9	- 8.3	1.4 ± 1.0 x 10^6
50	10.6	- 5.1 ± 1.3	14.1 ± 4.8	- 4.2	- 9.3	3.2 ± 0.6 x 10^7

Lipid/peptide ratios where NAPHT-BP100 is fully bound are related to the stoichiometry of positively charged lysine side chains in the peptide and the [POPG]. At a lipid/peptide ratio of ca. 10, the POPG/peptide ratio was five with LUV's containing equal amounts of POPC:POPG (**Table 3**). Under these conditions, the ratio between the number of negative charges in POPG and positive charges in the peptide is 1, and the system is electroneutral. With (70:30) POPC:POPG complete peptide binding occurs at a lipid/peptide ratio of ca. 21, a condition for electroneutrality.

3.4 Carboxyfluorescein leakage

BP100 and its analogs induce membrane permeabilization [17], and NAPHT-BP100 also causes CF leakage from lipid vesicles. Results are expressed in terms of lipid/peptide ratios because, as previously demonstrated [43], the extent of vesicle permeabilization depends on the peptide/lipid ratio.

NAPHT-BP100-induced membrane permeability increased with peptide concentration (**Figure 6 A and B**). At a lipid/peptide ratio of 10, condition which, according to binding studies (**Section 3.1, Figure 2 D**), all peptides were bound to POPC:POPG (50:50, molar ratio) LUV, the peptide caused 100% CF leakage (**Figure 6 C**).

Preprints (www.preprints.org) | NOT PEER-REVIEWED | Posted: 2 February 2021 doi:10.20944/preprints202102.0098.v1

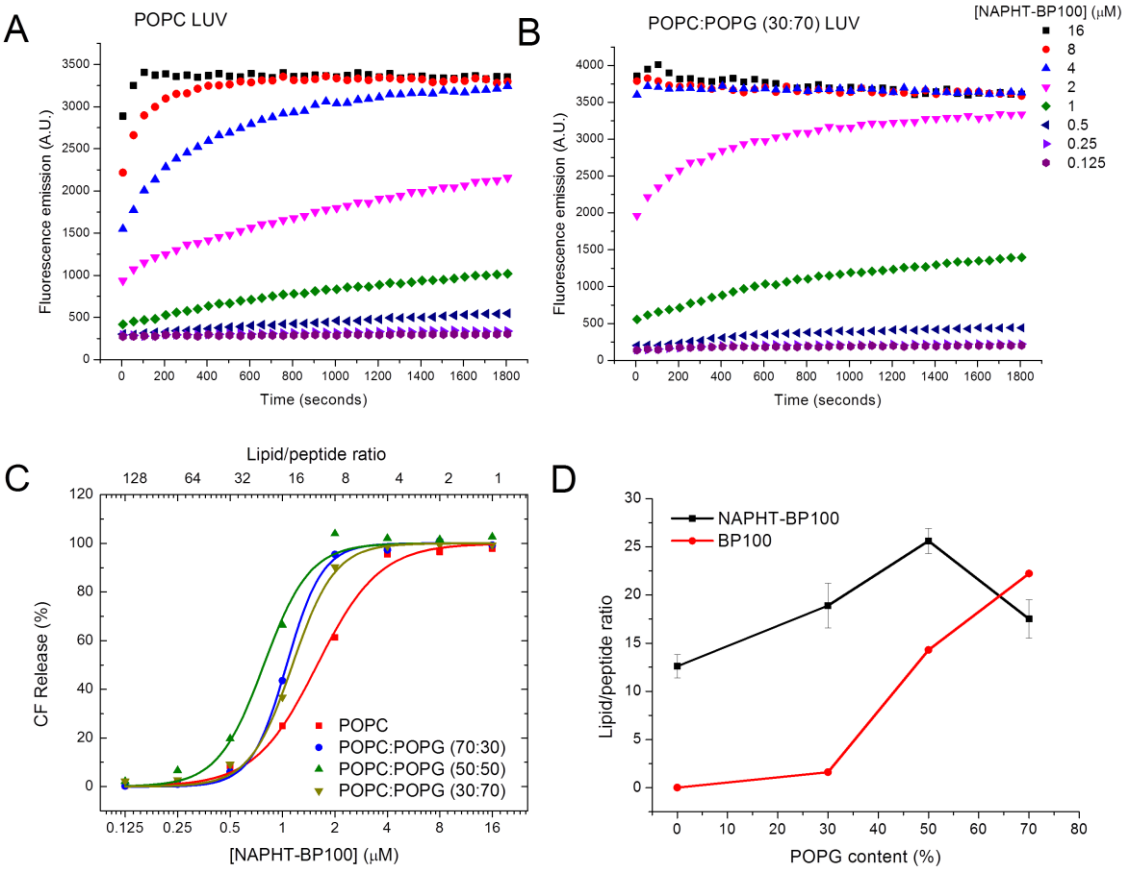

Figure 6. CF-induced leakage by NAPHT-BP100. Lipid concentration was 20 μM in Tris-HCl 10 mM, pH 7.4, with NaCl 300 mM. **(A)** POPC LUV, **(B)** POPC:POPG (30:70) LUV. **(C)** Percentage of CF release from LUV of varied lipid composition as a function of Napht-BP100, after 30 minutes. **(D)** Lipid/peptide ratio required to release 50% of CF from LUV as a function of POPG content. Measurements performed at 37 °C. BP100 data from Carretero et al. [17].

NAPHT-BP100 permeabilized POPC LUV, but the incorporation of POPG in LUV composition determined a greater leakage extent of leakage. Permeabilization extent and efficiency were analyzed by calculating the lipid/peptide ratio that caused 50% CF leakage (L/P_{50}). The Calculated L/P_{50} ratios increased with POPG (**Figure 6 D**). With a lipid/peptide ratio of 20, where NAPHT-BP100 is bound to LUV, the leakage extent increased from 24.9 to 43.6 and 66.4% by increasing the POPG content from 0 to 30 and 50 mol%. Lower permeabilization of POPC LUV confirmed both CD and fluorescence binding

Preprints (www.preprints.org) | NOT PEER-REVIEWED | Posted: 2 February 2021 doi:10.20944/preprints202102.0098.v1

results, which showed that NAPHT-BP100 interacts with a zwitterionic bilayer composed of POPC, although to a much lower extent when compared to POPG-containing membranes.

Comparing BP100 with NAPHT-BP100, it was clear that the additional alanine residues and naphthalimide increased the permeation effectiveness of NAPHT-BP100 and decreased the POPG-dependence for leaking.

3.5 DLS

NAPHT-BP100 triggered vesicle aggregation at peptide/lipid ratios above 0.12, and the apparent hydrodynamic diameter (Dh) increased to 1200 nm. The Dh increase was accompanied by an increase in the size distribution, as shown by the values of PdI and the measurement error (**Figure 7**).

Vesicle aggregation was correlated to the membrane net surface charge by analyzing Zeta potential (ZP) variations increasing peptide/lipid ratios (**Figure 7 B**). As previously reported for BP100 and other AMPs [17], vesicle aggregation is directly related to membrane charge neutralization caused by positively charged peptide binding to the negatively charged membrane. At a 0.12 peptide/lipid ratio, the membrane was neutral and, without vesicle-to-vesicle charge repulsion, LUV aggregated. Membrane surface charge varied from -35 mV to +20 mV when the peptide/lipid ratios changed between 0.10 and 0.15; beyond this point, added NAPHT-BP100 did not interact with vesicle aggregates, probably due to electrostatic repulsion, and no further Dh or ZP changes were observed (**Figure 7 B**).

Preprints (www.preprints.org) | NOT PEER-REVIEWED | Posted: 2 February 2021 doi:10.20944/preprints202102.0098.v1

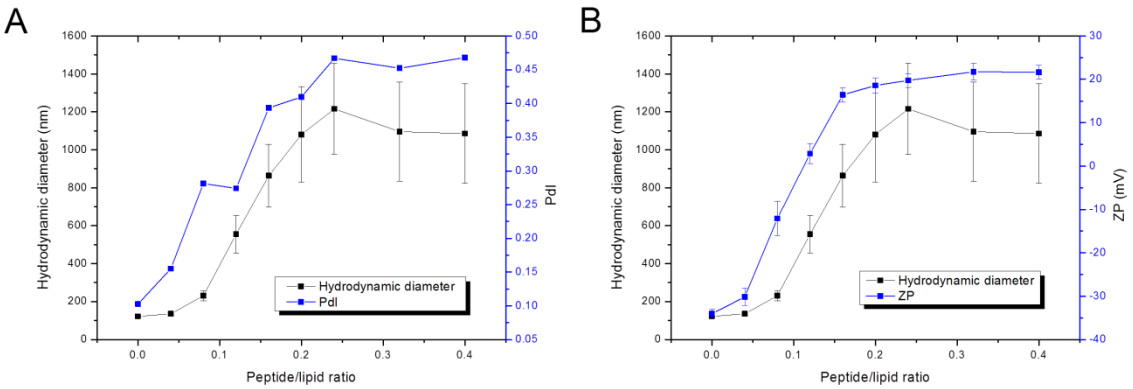

Figure 7. Effect of Peptide/lipid ratio on LUV's Dh and ZP. **(A)** Dh and polydispersity (PdI), and **(B)** Dh and ZP of POPC:POPG (50:50) LUV, as a function of peptide/lipid ratio. Lipid concentration was 50 µM in Tris-HF 10 mM, pH 7.4 buffer. Temperature was 25 °C.

3.6 Differential scanning calorimetry

DPPC: DPPG-mixed MLV exhibited a pre-transition (32.5 °C) from an Lβ′- to a Pβ′-phase (both gel phases), and the main transition at 40.9 °C to the liquid-crystalline Lα-phase (**Figure 8**). At this pH, DPPC and DPPG mixtures behave nearly ideally in both phases and, as evidenced by the narrow main transition, indicate a process of high cooperativity [44, 45].

Preprints (www.preprints.org) | NOT PEER-REVIEWED | Posted: 2 February 2021 doi:10.20944/preprints202102.0098.v1

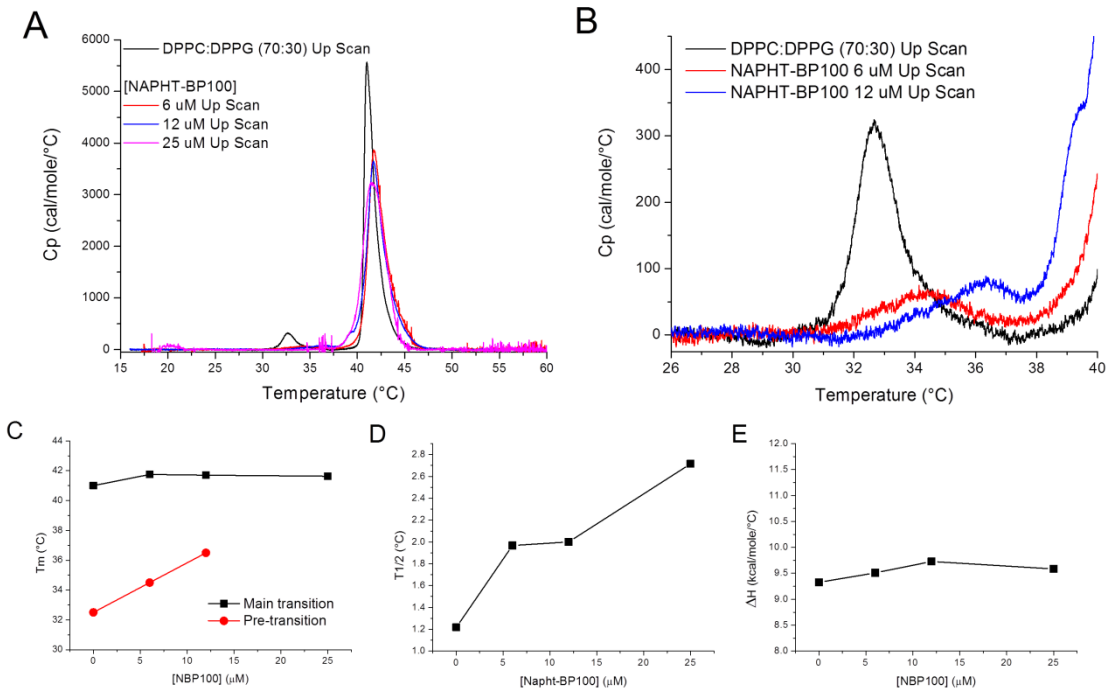

Figure 8. NAPHT-BP100 effects on lipid organization. Lipid concentration was 1.0 mM in Tris-HCl 10 mM, pH 7.4, buffer solution. **(A)** Differential scanning calorimetry heating scans of DPPC:DPPG (70:30, mol:mol) MLV in solution and with of various NAPHT-BP100 concentrations. **(B)** Expanded scale heating scans. **(C)** Main and pre-transition phase temperatures, **(D)** $\Delta T_{1/2}$ of main transition phase peak, and **(E)** phase transition enthalpy of MLV as a function of NAPHT-BP100 peptide concentration.

The pre-transition was up-shifted with 25 µM NAPHT-BP100 (lipid/peptide ratio 80) and superimposed with the main transition (**Figure 8 A, B, and C**). The addition of 6, 12, or 25 µM NAPHT-BP100 transition up-shifted the main transition by 0.7 °C (**Figure 8 A and C**), decreased the cooperativity and increased the value of $\Delta T_{1/2}$ (**Figure 8 A and D**). The phase transition enthalpy of DPPC:DPPG mixed vesicles at pH 7.4, was ~ 9 kcal/mol and peptide addition did not significantly modify this parameter significantly (**Figure 8 E**). The limited destabilization of the DPPC:DPPG gel phase by NAPHT-BP100 may be related to its interfacial position in the bilayer [8].

Preprints (www.preprints.org) | NOT PEER-REVIEWED | Posted: 2 February 2021 doi:10.20944/preprints202102.0098.v1

3.7 Minimum inhibitory concentration

The additional two alanine residues and the naphthalimide group linked to the BP100 sequence improved the peptide's ability for inhibit bacterial growth against *E. coli* and *S. aureus* and did not alter the activity against *B. subtilis* [17]. No exact correlation regarding improving activity and specie Gram stain could be drawn. The higher inhibitory activity of NAPHT-BP100, in comparison with BP100, correlates with NAPHT-BP100 greater membrane affinity and is related to NAPHT-BP100 ability to bind bacterial cytoplasmic DNA.

Table 4. MIC values for BP100 and NAPHT-BP100.

	BP100	**NAPHT-BP100**
E. coli	2 µM	1 µM
S. aureus	2 µM	1 µM
B. subitilis	2 µM	2 µM

3.8 Hemolytic activity

NAPHT-BP100 caused significant hemolysis above 8 µM (**Figure 9**). Compared to BP100 [17] (Fit projected C_{50} = 163 µM), NAPHT-BP100 displayed greater toxicity (C_{50} = 23 µM). This effect correlates with the higher membrane affinity of the peptide. Studies with the POPC zwitterionic model membrane, an adequate lipid membrane composition to correlate with neutral RBC cell membrane, showed that NAPHT-BP100 binds to and permeabilizes LUV to a greater extent than BP100.

Preprints (www.preprints.org) | NOT PEER-REVIEWED | Posted: 2 February 2021 doi:10.20944/preprints202102.0098.v1

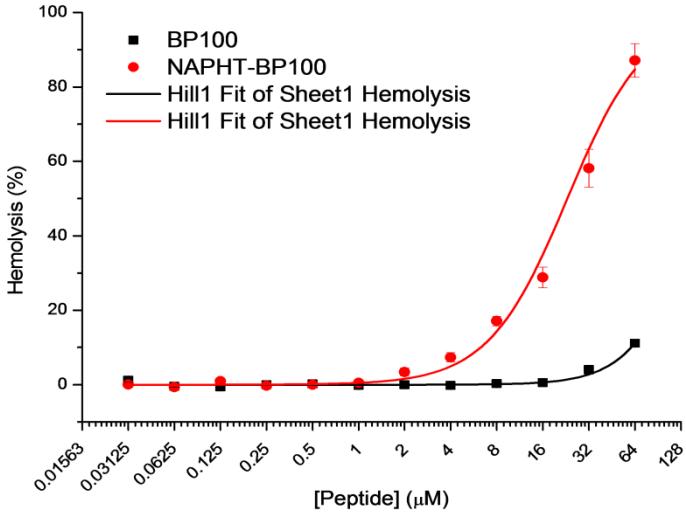

Figure 9. Hemolytic activity of BP100 (black) and NAPHT-BP100 (red) as function of peptide concentration. Red blood cells 1.5% (v/v) in PBS, pH 7.0. Temperature was 37 °C.

Preprints (www.preprints.org) | NOT PEER-REVIEWED | Posted: 2 February 2021 doi:10.20944/preprints202102.0098.v1

4. Discussion

The Synthesis, properties, and biological activities of amphiphilic peptides covalently linked to groups of diverse chemical structures are of fundamental and applied interest [3, 17, 46, 47].

Membrane-NAPHT-BP100 binding was extensively studied using different techniques (**Figures 2, 4 and 5, Tables 1 and 3**). Altogether, our results allowed the quantification of the binding extent and the measurement and description of the thermodynamic parameters of the interaction. The Fluorescence emission spectrum of the naphthalimidic group of the peptide varied both quantitatively and qualitatively as the LUV concentration increased (**Figure 2**). Non-substituted 1,8-naphthalimide presents higher quantum yields in polar protic solvents when compared to a hydrophobic aprotic environment [38]; thus, changes in emission can be attributed to fluorophore passage from the bulk solution to the more hydrophobic and less hydrated membrane surface environment. CD spectra of the peptide at different lipid concentrations also varied quantitatively and qualitatively (**Figure 4**), and. in this case, changes are attributed to conformational variations occurring as NAPHT-BP100 passes from the bulk solution to the membrane. CD and fluorescence binding data are in a good agreement and clearly indicate that NAPHT-BP100 is able to bind to POPC LUV to a low extent and the binding extent increases in a POPG content-dependent manner, highlighting the importance of electrostatic interaction between the positively charged lysine residue side chain and negatively charged phosphate groups of POPG. In comparison with BP100, NAPHT-BP100 presented higher affinity to the LUV and reduced charge dependence. The extra two alanine residues used as a spacer and the aromatic rings of the

Preprints (www.preprints.org) | NOT PEER-REVIEWED | Posted: 2 February 2021 doi:10.20944/preprints202102.0098.v1

naphthalimide moiety at the BP100 N-terminal increased molecular hydrophobicity and contributed to peptide-membrane interaction by decreasing the energy to accommodate the peptide on the bilayer hydrophilic/hydrophobic interface regardless of the membrane surface charge – NAPHT-BP100, differently from BP100, was able to bind to POPC LUV. Helix stabilization given by the addition of the alanine residues at the BP100 N-terminal sequence would also play an important role in increasing peptide-membrane interactions.

ITC data analysis allowed us confirmed that peptide-membrane interaction is essentially driven by electrostatic interactions (**Figure 5, Table 3**), as shown by CD and fluorescence results. The Measured negative enthalpy variation is mostly associated with charge neutralization. The role of electrostatic interaction was made even clearer as the calculated stoichiometry of the interaction is essentially given by one molecule of POPG to one lysine side chain of the peptide, as demonstrated (**Table 3**).

The main phenomena associated with entropy variation are peptide dehydration and secondary structure acquisition as well as the hydrophobic effect driving the interaction between the α-helix non-polar face and lipid acyl chains. Although helix acquisition represents a configurational entropy loss, peptide dehydration and hydrophobic effects increase the overall entropy, resulting in a significant energetic contribution in the total free energy variation.

The secondary structure in water bound to the LUV was investigated by CD (**Figure 4, Table 2**). CD spectra showed that the peptide undergoes a coil to an α-helix upon binding to LUV containing POPG.

Preprints (www.preprints.org) | NOT PEER-REVIEWED | Posted: 2 February 2021 doi:10.20944/preprints202102.0098.v1

In solution, NAPHT-BP100 presents a small content of α-helix (19 %, or 2.5 residues) and is essentially in a flexible random conformation (81 %, or 10.5 residues) (**Figure 4, Table 2**). The small but significant content of the α-helix secondary structure is most likely an effect of the Napht-Ala-Ala segment attached to the BP100 sequence since, in solution, BP100 is completely in random conformation [8, 14, 15, 16]. As reported, the addition of chemical groups to the BP100 N-terminal affected its structure in water by enhancing the content of α-helix [17] and alanine residues are known to play a role as α-helix stabilizers [49].

Binding to lipid bilayers containing POPG triggered the acquisition of an α-helical structure (80 %, or 10.4 residues) (**Figure 4, Table 2**). Conformational changes are directly related to peptide dehydration occurring as peptides interacts more closely with the bilayer surface, and to the lower availability of water molecules in the membrane surface that trigger the establishment of intermolecular hydrogen bonds in the peptide that adopts an α-helical secondary structure [8, 50]. Helical wheel projection and theoretical calculations of NAPHT-BP100 indicate that the peptide, BP100, forms an amphipathic α-helix with two extra alanine residues attached to the N-terminal end lying in the hydrophobic face of the structure [51] (**Figure 10**). According to the Eisenberg plot [52], NAPHT-BP100 the overall hydrophobicity (<H> = 0.409) and significant hydrophobic moment (<μH> = 0.737) classify the peptide-formed helix as a membrane surface seeking. In addition, it has been reported that slight variations in peptide sequence, thus in its hydrophobicity and hydrophobic moment, can trigger considerable changes in peptide-membrane interaction and permeabilizing capabilities of the peptide [53, 54].

Preprints (www.preprints.org) | NOT PEER-REVIEWED | Posted: 2 February 2021 doi:10.20944/preprints202102.0098.v1

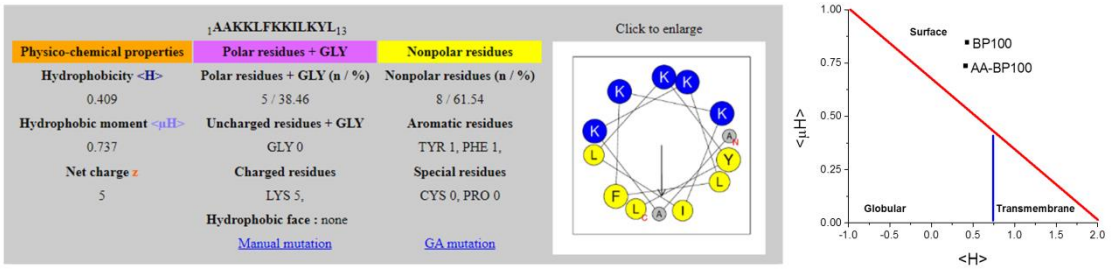

Figure 10. (A) NAPHT-BP100 peptide sequence and formed α-helix properties calculated using Heliquest [51]. **(B)** BP100 and NAPHT-BP100 α-helices properties placed in Eisenberg plot.

Changes in liposome size and size distribution, and zeta potential triggered by NAPHT-BP100 were measured using dynamic light scattering (**Figure 7**), revealing that membrane charge neutralization plays an important role in membrane destabilization, ultimately causing liposome aggregation. The relationship between liposome charge neutralization and interaction stoichiometry could be detailed by zeta potential measurements, indicating that most of the peptide effect occurs in the lipid to peptide ratio range in which the Zeta potential is close to 0 mV and the sample has approximately one molecule of POPG to each lysine side chain of the peptide. This observation corroborates the stoichiometry calculated from ITC data (**Table 3**) and brings relevant information regarding NAPHT-BP100 mechanism of action, suggesting a detergent-like mechanism in which charge neutralization triggers LUV aggregation and complete disruption.

The analysis of the secondary structure amphipathic profile indicated that the peptide tends to occupy an interfacial position in the bilayer, and, in agreement with the predicted, DSC experiments showed that the peptide does not cause a major effect on gel phase lipid organization, supporting the proposed shallow penetration (**Figure 8**). Thermodynamic lipid phase transition parameters of

Preprints (www.preprints.org) | NOT PEER-REVIEWED | Posted: 2 February 2021 doi:10.20944/preprints202102.0098.v1

DPPC:DPPG (70:30) MLV and the effect of the peptide on these parameters were examined by differential scanning calorimetry (**Figure 8**). essentially, no significant influence was observed, especially regarding the overall process energy and the main transition temperature.

CF leakage assays to test peptide efficiency for permeabilizing LUV were evaluated considering the binding extent and structure of the peptide in the bilayer, the bilayer surface charge neutralization and the low effect of the peptide on lipid acyl chains (**Figure 6**). Interestingly, peptide activity efficiency followed the previously measured binding extent in terms of both lipid/peptide ratio and LUV POPG content. Although low binding of NAPHT-BP100 to POPC LUV was demonstrated, the peptide was able to bind and cause CF leakage from these liposomes, confirming the presence and relevance of hydrophobic interactions and other phenomena not associated with electrostatic interactions.

The Measured biological activity of NAPHT-BP100 against bacteria and human RBC corroborates the series of biophysical studies discussed so far. Experiments with POPG containing LUV, especially at 30 mol%, mimicking PG molar concentrations found in bacteria, were correlated with the MIC results. Observations taken in experiments with zwitterionic POPC LUV were correlated to the biological hemolytic activity assay considering the human RBC neutral membrane surface. In comparison with BP100, NAPHT-BP100 showed higher affinity to all studied LUV compositions, resulting in a higher effect on the membrane regardless of its composition. These observations can be translated to the observed greater biological activity of NAPHT-BP100 against *E. coli* and *S. aureus*, confirmed by the measured lower MIC values (**Table 4**), and to greater toxicity against human RBC as demonstrated by the hemolysis test

Preprints (www.preprints.org) | NOT PEER-REVIEWED | Posted: 2 February 2021 doi:10.20944/preprints202102.0098.v1

(**Figure 9**). Increased activity of NAPHT-BP100 against *E. coli* and *S. aureus* could also relate to the internalization of NAPHT-BP100 into the bacteria and NAPHT-BP100-ds-DNA interaction, resulting in DNA replication and RNA transcription blockage. NAPHT-BP100 bound to a large extent to ds-DNA (**Figure 3**) and naphthalimide derivatives are known to be able to intercalate between ds-DNA base pairs that affect a series of related cellular processes [27].

The increase in hydrophobicity and hemolytic activity of NAPHT-BP100 was balanced by its improved antibacterial action and did not change to a large extent peptide therapeutic index. The indication that NAPHT-BP100 could act upon the bacteria not only by destabilizing its membrane but also by binding the cell ds-DNA, meaning the possibility to act by more than a single mechanism, would also consist in a considerable improvement in terms of avoiding bacterial resistance. Although more hemolytic, NAPHT-BP100 can be applied to the design of antibacterial molecules targeting various types of cutaneous or other mucosal infections. In this context, the results found in the present work can provide subsidies for studies aimed at drug development.

 doi:10.20944/preprints202102.0098.v1

5. References

[1] C. Chen and T. Lu, "Development and Challenges of Antimicrobial Peptides for Therapeutic Applications," *Antibiotics,* vol. 9, no. 1, p. 24, 2020.

[2] K. Lohner, "Membrane-active antimicrobial peptides as template structures for novel antibiotic agents," *Curr. Top. Med. Chem.,* vol. 17, no. 5, pp. 508-519, 2017.

[3] J. Li, J. J. Koh, S. Liu, R. Lakshminarayanan, C. S. Verma and R. W. Beuerman, "Membrane active antimicrobial peptides: Translating mechanistic insights to design," *Frontiers in Neurosciences,* vol. 11, p. 73, 2017.

[4] H. Jenssen, P. Hamill and R. E. W. Hancock, "Peptide antimicrobial agents," *Clinical Microbiology Reviews,* vol. 19, no. 3, pp. 491-511, 2006.

[5] L. Nguyen, E. Haney and H. Vogel, "The expanding scope of antimicrobial peptide structures and their modes of action," *Trends in Biotechnology,* vol. 29, no. 9, pp. 464-472, 2011.

[6] J. Powers and R. Hancock, "The relationship between peptide structure and antibacterial activity," *Peptides,* vol. 24, no. 11, pp. 1681-1691, 2003.

[7] M. Yeaman and N. Yount, "Mechanisms of antimicrobial peptide action and resistance," *Pharmacological Reviews,* vol. 55, no. 1, pp. 27-55., 2003.

[8] P. Park, L. R. Franco, H. Chaimovich, K. R. Coutinho, I. M. Cuccovia and F. S. Lima, "Binding and flip as initial steps for BP-100 antimicrobial actions," *Scientific Reports,* vol. 9, p. 8622, 2019.

[9] J. Killian and G. von Heijne, "How proteins adapt to a membrane-water interface," *Trens in Biochemical Sciences,* vol. 25, no. 9, pp. 429-434, 2000.

[10] F. Lima, M. Andrade, L. Mortara, L. Dias, I. Cuccovia and H. Chaimovich, "Ion dehydration controls adsorption at the micellar interface: hydrotropic ions," *Physical Chemistry Chemical Physics,* vol. 19, no. 45, pp. 30658-30666, 2017.

[11] E. Badosa, R. Ferre, M. Planas, L. Feliu, E. Besalú, J. Cabrefiga, E. Bardají and E. Montesinos, "A library of linear undecapeptides with bactericidal activity against phytopathogenic bacteria," *Peptides,* vol. 28, no. 12, p. 2276–2285, 2007.

[12] R. Ferre, M. N. Melo, A. D. Correia, L. Feliu, E. Bardají, M. Planas and M. Castanho, "Synergistic effects of the membrane actions of cecropin-melittin antimicrobial hybrid peptide BP100," *Biophysical journal,* vol. 96, no. 5, pp. 1815-1827, 2009.

[13] C. S. Alves, M. N. Melo, H. G. Franquelim, R. Ferre, M. Planas, L. Feliu, E. Bardají, W. Kowalczyk, D. Andreu, N. C. Santos, M. X. Fernandes and M. Castanho, "Escherichia coli cell surface perturbation and disruption induced by antimicrobial peptides BP100 and pepR," *Journal of Biological Chemistry,* vol. 285, no. 36, pp. 27536-27544, 2010.

[14] I. Torcato, Y. Huang, H. Franquelim, D. Gaspar, D. Craik, M. Castanho and S. Troeira-Henriques, "Design and characterization of novel antimicrobial peptides, R-BP100 and RW-BP100, with activity against Gram-negative and Gram-positive bacteria," *Biochimica et Biophysica Acta - Biomembranes,* vol. 1828, no. 3, pp. 944-955, 2013.

[15] M. Manzini, K. Perez, K. Riske, J. Bozelli, T. Santos, M. Da Silva, G. Saraiva, M. Politi, A. Valente, F. Almeida, H. Chaimovich, M. Rodrigues, M. Bemquerer, S. Schreier and I. Cuccovia, "Peptide:lipid ratio and membrane surface charge determine the mechanism of action of the antimicrobial peptide BP100. Conformational and functional studies," *Biochimica et Biophysica Acta - Biomembranes,* vol. 1838, no. 7, pp. 1985-1999, 2014.

[16] P. Wadhwani, E. Strandberg, J. Van Den Berg, C. Mink, J. Bürck, R. Ciriello and A. Ulrich, "Dynamical structure of the short multifunctional peptide BP100 in membranes," *Biochimica et Biophysica Acta - Biomembranes,* vol. 1838, no. 3, pp. 940-949, 2014.

[17] G. Carretero, G. Saraiva, A. Cauz, M. K. S. Rodrigues, K. Riske, A. dos Santos, M. Pinatto-Botelho, M. Bemquerer, F. Gueiros-Filho, H. Chaimovich, S. Schreier and I. Cuccovia, "Synthesis, biophysical and functional studies of two BP100 analogues modified by a hydrophobic chain and a cyclic peptide," *Biochimica et Biophysica Acta - Biomembranes,* vol. 1860, no. 8, pp. 1502-1516, 2018.

[18] B. Zhang, H. Gu, W. Shi, H. Li, G. Ma, X. Chen, H. Qian, H. Lin, W. Huang and L. Ge, "Synthesis and biological evaluation of novel aliphatic acid-conjugated antimicrobial peptides as potential agents with anti-tumor, multidrug resistance-reversing activity and enhanced stability," *Amino Acids,* vol. 49, no. 11, pp. 1831-1841, 2017.

[19] A. Kamal, N. Bolla, P. Srikanth and A. Srivastava, "Naphthalimide derivatives with therapeutic characteristics: a patent review," *Expert opinion*

 doi:10.20944/preprints202102.0098.v1

on therapeutic patents, vol. 23, no. 3, p. 299–317, 2013.

[20] M. Braña and A. Ramos, "Naphthalimides as anti-cancer agents: synthesis and biological activity," *Current Medicinal Chemistry - Anti-Cancer Agents,* vol. 1, no. 3, pp. 237-255, 2001.

[21] L. Min and X. Hui, "Overview of Naphthalimide Analogs as Anticancer Agents," *Current Medicinal Chemistry,* vol. 16, no. 36, pp. 4797-4813, 2009.

[22] L. Ingrassia, F. Lefranc, R. Kiss and T. Mijatovic, "Naphthalimides and Azonafides as Promising Anti-Cancer Agents," *Current Medicinal Chemistry,* vol. 16, no. 10, pp. 1192-213, 2009.

[23] R. Tandon, J. Luxami, H. Kaur, N. Tandon e K. Paul, “1,8-Naphthalimide: A Potent DNA Intercalator and Target for Cancer Therapy,” *The Chemical Record,* vol. 10, n. 17, pp. 956-993, 2017.

[24] J. Kang, L. Gopala, V. Reddy-Tangadanchu, W. Gao and C. H. Zhou, "Novel naphthalimide nitroimidazoles as multitargeting antibacterial agents against resistant Acinetobacter baumanni," *Future Medicinal Chemistry,* vol. 10, no. 7, pp. 711-724, 2018.

[25] M. Marinov, I. Kostova, E. Naydenova and N. Stoyanov, "Synthesis and antimicrobial activity of 1,8-naphthalimide derivatives of nalidixic acid," *Journal of Chemical Technology and Metallurgy,* vol. 54, no. 6, pp. 1146-1156, 2019.

[26] H. Shaki, A. Khosravi, J. Gharanjig and A. Mahboubi, "Investigation of synthesis, characterization, photophysical and biological properties of novel antimicrobial fluorescent naphthalimide derivatives," *Materials Technology, 2016. 31(6): p. 322-331.,* vol. 31, no. 6, pp. 322-331, 2016.

[27] S. Banerjee, E. Veale, C. Phelan, S. Murphy, G. Tocci, L. Gillespie, D. Frimannsson, J. Kelly and T. Gunnlaugsson, "Recent advances in the development of 1,8-naphthalimide based DNA targeting binders, anticancer and fluorescent cellular imaging agents," *Chem. Soc. Rev.,* vol. 42, pp. 1601-1618, 2013.

[28] S. Hickey, T. Ashton, G. Boer, C. Bader, M. Thomas, A. Elliott, C. Schmuck, H. Yu, J. Li, R. Nation, M. Cooper, S. Plush, D. Brooks and F. Pfeffer, "Norbornane-based cationic antimicrobial peptidomimetics targeting the bacterial membrane," *European journal of medicinal chemistry,* vol. 160, pp. 9-22, 2018.

 doi:10.20944/preprints202102.0098.v1

[29] A. Wu, Y. Xu and X. Qian, "Novel naphthalimide-amino acid conjugates with flexible leucine moiety as side chain: design, synthesis and potential antitumor activity.," *Bioorganic & medicinal chemistry,* vol. 17, no. 2, pp. 592-599, 2009.

[30] W. Chan and P. White, FMOC Solid Phase Peptide Synthesis, Oxford University Press, 2000.

[31] M. Friedman, "Applications of the ninhydrin reaction for analysis of amino acids, peptides, and proteins to agricultural and biomedical sciences," *Journal of Agricultural and Food Chemistry,* vol. 52, no. 3, pp. 385-406, 2004.

[32] B. Abraham and L. Kelly, "Photooxidation of Amino Acids and Proteins Mediated by Novel 1,8-Naphthalimide Derivatives," *Journal of Physical Chemistry B,* vol. 107, no. 45, pp. 12534-12541, 2003.

[33] B. Aveline, S. Matsugo and R. Redmond, "Photochemical Mechanisms Responsible for the Versatile Application of Naphthalimides and Naphthaldiimides in Biological Systems," *Journal of the American Chemical Society,* vol. 119, no. 49, pp. 11785-11795, 1997.

[34] M. Shibue, C. Mant and R. Hodges, "Effect of anionic ion-pairing reagent concentration (1-60 mM) on reversed-phase liquid chromatography elution behaviour of peptides," *Journal of Chromatography A,* vol. 1080, no. 1, pp. 58-67, 2005.

[35] G. Rouser, S. Fleischer and A. Yamamoto, "Two dimensional thin layer chromatographic separation of polar lipids and determination of phospholipids by phosphorus analysis of spots," *Lipids,* vol. 5, no. 5, pp. 494-496, 1970.

[36] I. Wiegand, K. Hilpert and R. Hancock, "Agar and broth dilution methods to determine the minimal inhibitory concentration (MIC) of antimicrobial substance. , 2008. 3: p. 163-75.," *Nature protocols,* vol. 3, pp. 163-175, 2008.

[37] B. Mojsoska, G. Carretero, S. Larsen, R. Mateiu and H. Jenssen, "Peptoids successfully inhibit the growth of gram negative E. coli causing substantial membrane damage," *Scientific Reports,* vol. 7, p. 42332, 2017.

[38] J. Magalhães, R. Pereira, E. Triboni, P. Berci Filho, M. Gehlen and F. Nart, "Solvent effect on the photophysical properties of 4-phenoxy-N-methyl-1,8-naphthalimide," *Journal of Photochemistry and Photobiology A: Chemistry,*

 doi:10.20944/preprints202102.0098.v1

vol. 183, no. 1, pp. 165-170, 2006.

[39] S. Banerjee, J. Kitchen, T. Gunnlaugsson and J. Kelly, "Synthesis and photophysical evaluation of a pyridinium 4-amino-1,8-naphthalimide derivative that upon intercalation displays preference for AT-rich double-stranded DNA," *Org. Biomol. Chem.,* vol. 10, pp. 3033-3043, 2012.

[40] J. Misiewicz, S. Afonin, S. Grage, J. Van Den Berg, E. Strandberg, P. Wadhwani and A. Ulrich, "Action of the multifunctional peptide BP100 on native biomembranes examined by solid-state NMR," *Journal of Biomolecular NMR, 2015. 61(3): p. 287-298,* vol. 61, no. 3, pp. 287-298, 2015.

[41] A. Micsonai, F. Wien, É. Bulyáki, J. Kun, É. Moussong, Y. H. G. Y. Lee, M. Réfrégiers and J. Kardos, "BeStSel: a web server for accurate protein secondary structure prediction and fold recognition from the circular dichroism spectra.," *Nucleic acids research,* vol. 46, no. W1, pp. W315-W322, 2018.

[42] L. Mortara, H. Chaimovich, I. Cuccovia, D. Horinek and F. Lima, "Dehydration Determines Hydrotropic Ion Affinity for Zwitterionic Micelles," *Journal of Chemical Information and Modeling,* vol. 60, no. 2, pp. 604-610, 2020.

[43] A. Cauz, G. Carretero, G. Saraiva, P. Park, L. Mortara, I. Cuccovia, M. Brocchi and F. Gueiros-Filho, "Violacein targets the cytoplasmic membrane of bacteria," *ACS Infectious Diseases,* vol. 5, no. 4, pp. 539-549, 2019.

[44] P. Garidel, C. Johann, L. Mennicke and A. Blume, "The mixing behavior of pseudobinary phosphatidylcholine-phosphatidylglycerol mixtures as a function of pH and chain length," *European Biophysics Journal,* vol. 26, no. 6, pp. 447-459, 1997.

[45] A. Hildebrand, K. Beyer, R. Neubert, P. Garidel and A. Blume, "Solubilization of negatively charged DPPC/DPPG liposomes by bile salts," *Journal of colloid and interface science,* vol. 279, no. 2, pp. 559-571, 2006.

[46] K. Eggenberger, C. Mink, P. Wadhwani, A. Ulrich and P. Nick, "Using the peptide Bp100 as a cell-penetrating tool for the chemical engineering of actin filaments within living plant cells," *ChemBioChem,* vol. 12, no. 1, pp. 132-137, 2011.

[47] A. Reinhardt and I. Neundorf, "Design and Application of Antimicrobial Peptide Conjugates," *International journal of molecular sciences,* vol. 17,

 doi:10.20944/preprints202102.0098.v1

no. 5, p. 701, 2016.

[48] H. Zamora-Carreras, E. Strandberg, P. Mühlhäuser, J. Bürck, P. Wadhwani, M. Jiménez, M. Bruix and A. Ulrich, "Alanine scan and 2H NMR analysis of the membrane-active peptide BP100 point to a distinct carpet mechanism of action," *Biochimica et Biophysica Acta - Biomembranes,* vol. 1858, no. 6, pp. 1328-1338, 2016.

[49] C. Rohl, W. Fiori and R. Baldwin, "Alanine is helix-stabilizing in both template-nucleated and standard peptide helices," *Proceedings of the National Academy of Sciences,* vol. 96, no. 7, pp. 3682-3687, 1999.

[50] P. Almeida, A. Ladokhin and S. White, "Hydrogen-bond energetics drive helix formation in membrane interfaces," *Biochimica et Biophysica Acta,* vol. 1818, no. 2, pp. 178-182, 2012.

[51] R. Gautier, D. Douguet, B. Antonny and G. Drin, "HELIQUEST: a web server to screen sequences with specific α-helical properties," *Bioinformatics,* vol. 24, no. 18, pp. 2101-2102, 2008.

[52] D. Eisenberg, E. Schwarz, M. Komaromy and R. Wall, "Analysis of membrane and surface protein sequences with the hydrophobic moment plot," *Journal of Molecular Biology,* vol. 179, no. 1, pp. 125-142, 1984.

[53] G. Carretero, E. Vicente, E. Cilli, C. Alvarez, H. Jenssen and S. Schreier, "Dissecting the mechanism of action of actinoporins. Role of the N-terminal amphipathic α-helix in membrane binding and pore activity of sticholysins I and II," *PloS one,* vol. 13, no. 8, p. 0202981, 2018.

[54] U. Ros, G. Carretero, J. Paulino, E. Crusca, P. F. Jr, E. Cilli, M. Lanio, S. Schreier and C. Alvarez, "Self-association and folding in membrane determine the mode of action of peptides from the lytic segment of sticholysins," *Biochimie,* vol. 156, pp. 109-117, 2019.

Preprints (www.preprints.org) | NOT PEER-REVIEWED | Posted: 2 February 2021 doi:10.20944/preprints202102.0098.v1

Supplementary material

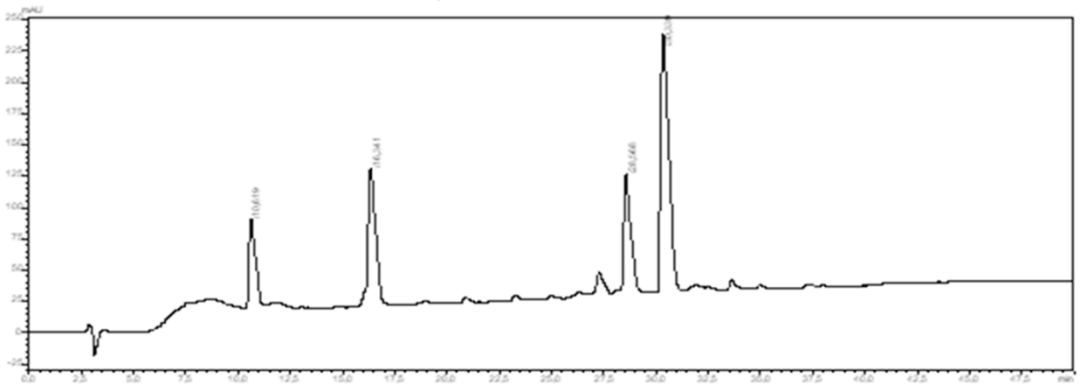

Figure SM-1. Analytical chromatographic profile of freeze dried crude Naphthalimide-AA-BP100 - 2 mg/mL in water; sample volume: 20 µL; analytical reversed-phase C18 Vydac column; solvent A: 0.1% TFA in water; solvent B: 80% aqueous acetonitrile containing 0.09 % TFA; gradient: 30-70 % B in 30 min; flow rate: 1 mL/min: detection wavelength: 220 nm. This peptide was constituted by four fractions which were separated from each other and purified separately using a preparative reversed-phase C18 Vydac column at flow rate: 9 mL/min; in the same experimental conditions of solvent and gradient above. Mass spectra analyses of each fractions indicated that peak 4 was the desired peptide ([M+H]+ = 1743.1).

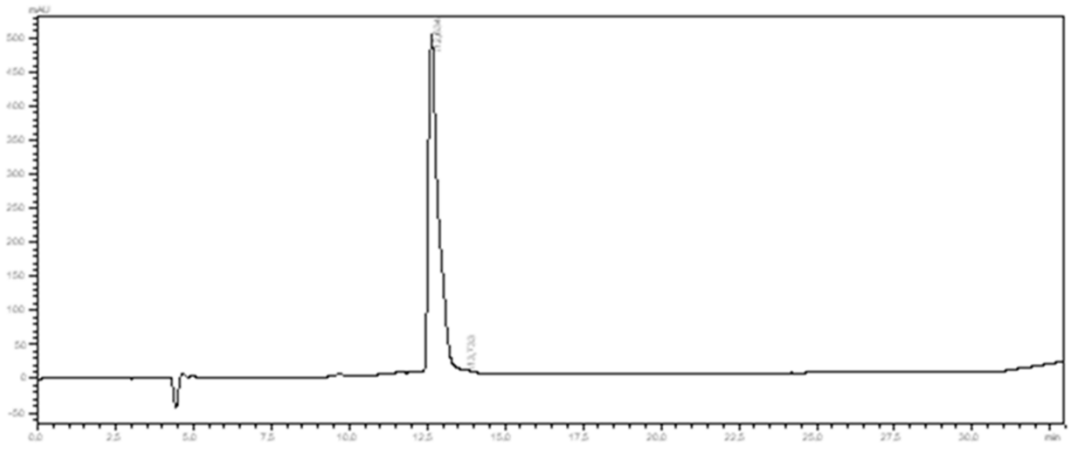

Figure SM-2. Analytical chromatographic profile of purified Naphthalimide-AA-BP100 (peak 4)- 2 mg/mL in water; sample volume: 20 uL, analytical reversed-phase C18 Vydac column; solvent A: 0.1% TFA in water; solvent B: 80% aqueous acetonitrile containing 0.09 % TFA; gradient: 30-40%B in 5 min plus 40-50%B in 20 min; flow rate: 1 mL/min: detection wavelength: 220 nm. HPLC purity grade: >99 %.

Preprints (www.preprints.org) | NOT PEER-REVIEWED | Posted: 2 February 2021 doi:10.20944/preprints202102.0098.v1

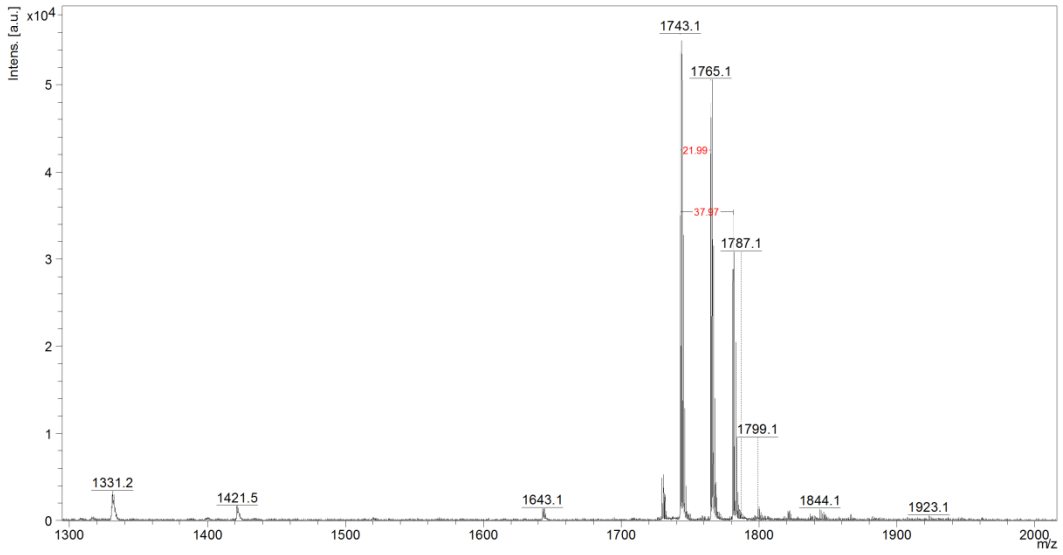

Figure SM-3. MALDI mass spectra of the purified peptide Naphthalimide-AA-BP100, showing the expected product with $[M+H]^+$= 1743.1 and the $[M+Na]^+$ and $[M+K]^+$ adducts at 1765.1 1nd 1787.1, respectively. Ions observed at *m/z* values of 1331.2, 1421.5 and 1643.1 might be due to partial in-source peptide fragmentation. The spectrum was obtained in an Autoflex Speed mass spectrometer (Bruker Daltonics, Bilerica, MA).

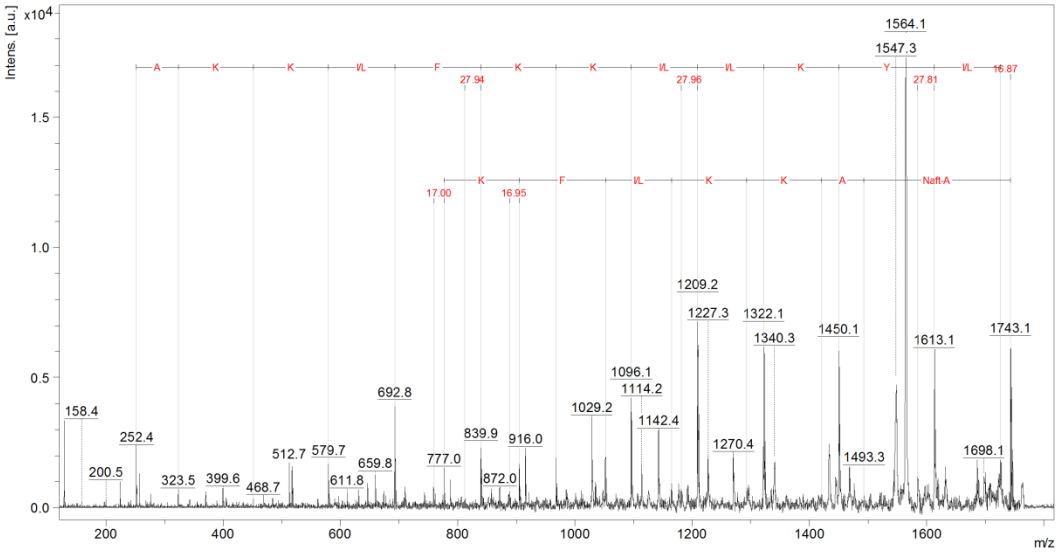

Figure SM-4. MS/MS spectrum of the peptide Naphthalimide-AA-BP100. The complete sequence obtained by the b ion-series is shown in the upper part whereas a partial sequence assigned by the y ion-series is shown below the b-series. The spectrum was obtained in an Autoflex Speed mass spectrometer (Bruker Daltonics, Bilerica, MA).

Preprints (www.preprints.org) | NOT PEER-REVIEWED | Posted: 2 February 2021 doi:10.20944/preprints202102.0098.v1

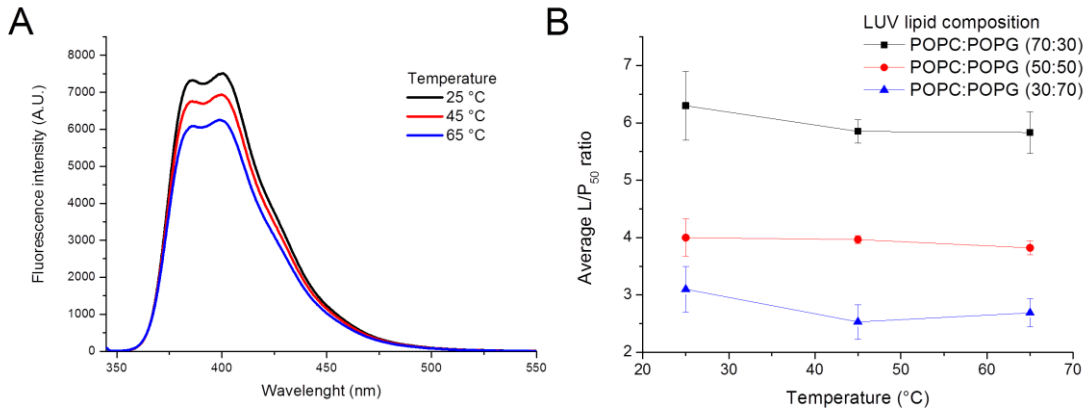

Figure SM-5. (A) Fluorescence spectra of NAPHT-BP100 20 µM in solution at 25, 45 and 65 °C in Tris-HCl 10 mM, pH 7.4 buffer. **(B)** Average lipid/peptide ratio in which 50% of NAPHT-BP100 is bound to LUV of varied lipid composition at 25, 45, and 65 °C.

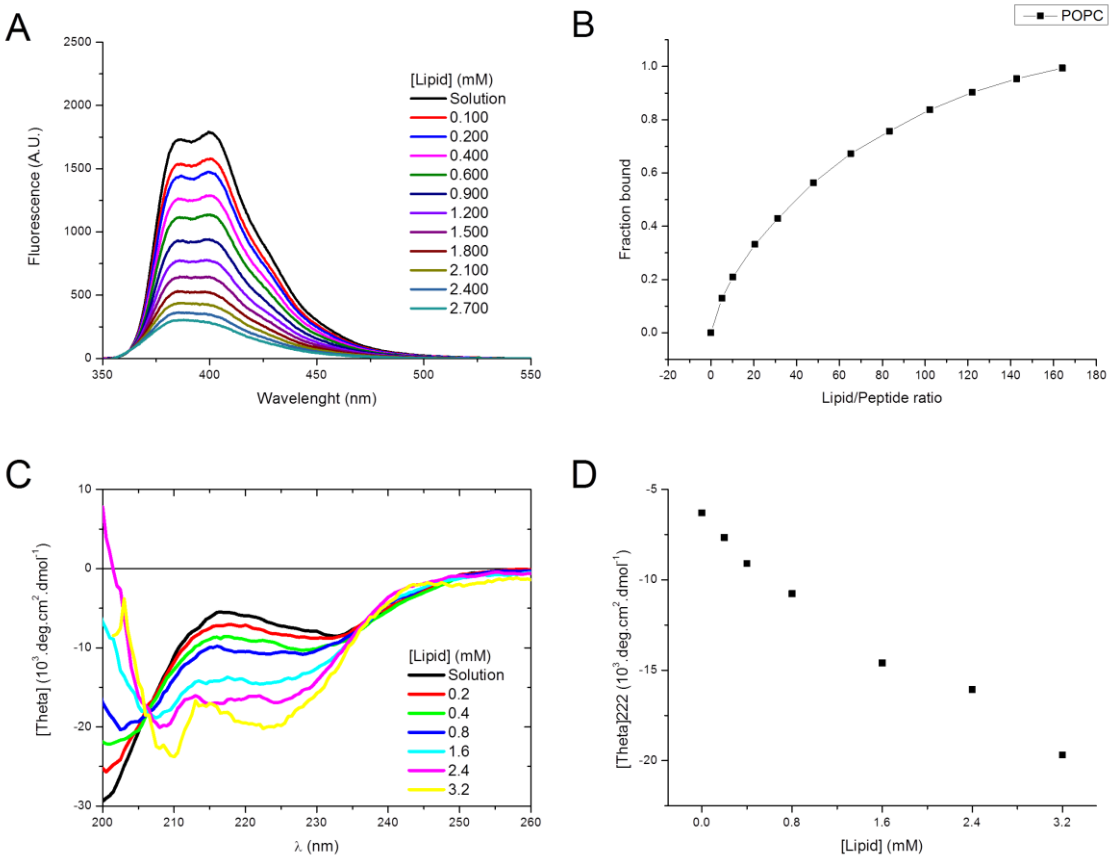

Figure SM-6. (A) Fluorescence and **(C)** CD spectra of NAPHT-BP100 20 µM in solution and in presence of POPC LUV, in Tris-HCl 10 mM, pH 7.4 buffer. **(B)** Binding isotherm obtained from the spectra presented in (A) and **(D)** [θ] at 222 nm as function of lipid concentration obtained from data in (C).